


Thickness dependence of magnetization reversal and magnetostriction in $\text{Fe}_{81}\text{Ga}_{19}$ thin films

W. Jahjah,¹ R. Manach,¹ Y. Le Grand,¹ A. Fessant,¹ B. Warot-Fonrose,² A.R.E. Prinsloo,³
C.J. Sheppard,³ D.T. Dekadjevi,^{1,3} D. Spenato,¹ and J.-Ph. Jay^{1,*}

¹Laboratoire d'Optique et de Magnétisme (OPTIMAG), EA 938, IBSAM, Université de Bretagne Occidentale, Brest 29200, France

²Nanomaterials Group - CEMES CNRS-UPR 8011, Université de Toulouse, Toulouse 31055, France

³Department of Physics, Cr Research Group, University of Johannesburg, P.O. Box 524, Auckland Park 2006, South Africa

 (Received 26 March 2019; revised manuscript received 14 June 2019; published 12 August 2019)

Among the magnetostrictive alloys, the one formed of iron and gallium (called “Galfenol” from its U.S. Office of Naval Research discoverers in the late 1990s) is attractive for its low hysteresis, good tensile stress, good machinability, and its rare-earth-free composition. One of its applications is its association with a piezoelectric material to form an extrinsic multiferroic composite as an alternative to the rare room-temperature intrinsic multiferroics such as BiFeO_3 . This study focuses on thin $\text{Fe}_{0.81}\text{Ga}_{0.19}$ films of thickness 5, 10, 20, and 60 nm deposited by sputtering onto glass substrates under a deposition field $H_{\text{dep}} \sim 300$ Oe. Magnetization reversal study reveals a well-defined symmetry with two principal directions independent of the thickness. The magnetic signature of this magnetic anisotropy decreases with increasing $\text{Fe}_{81}\text{Ga}_{19}$ thickness due to an increase of the nonpreferential polycrystalline arrangement, as revealed by transmission electron microscopy (TEM) observations. Thus, when magnetic field is applied along these specific nontrivial directions, magnetization reversal is mainly coherent for the thinnest sample, as seen from the transverse magnetization cycles. The magnetostriction coefficient reaches 20 ppm for the 5-nm film and decreases for thicker samples, where the polycrystalline part with nonpreferential orientation prevails.

DOI: [10.1103/PhysRevApplied.12.024020](https://doi.org/10.1103/PhysRevApplied.12.024020)

I. INTRODUCTION

Magnetostrictive thin films have attracted a huge interest in the last few decades. Indeed, it is of interest to understand the fundamental mechanisms driving the strain and magnetic coupling in thin films. Also, magnetostrictive properties are the key properties used in different applied issues and devices such as sensors, actuators, energy-harvesters, spintronic devices [1,2], and straintronic devices [3,4]. For example, a new technology, called acoustically assisted magnetic recording (AAMR) based on Fe-Ga alloy has been recently proposed. This technology uses a surface acoustic wave (SAW) to modulate the coercivity of the recording medium by the inverse magnetostrictive effect [5].

Among the different magnetostrictive alloys, Fe-Ga alloy discovered in 2000 by Clark [6] has received particular attention as it exhibits remarkable properties such as low hysteresis, large magnetostriction, good tensile strength, machinability, and recent progress in

commercially viable methods of processing [7]. Although Fe-Ga alloy magnetostrictive properties are lower than those of Terfenol-D (a terbium-iron-dysprosium alloy), gallium, when substituted for iron, increases the tetragonal magnetostriction coefficient λ_{100} over tenfold. This increase is generally attributed to the formation of Ga pairs when the Ga concentration reaches a substitution concentration value of 19% Ga, whereas it is commonly believed that the formation of an ordered DO_3 phase, as the alloy composition approaches 25% Ga, is detrimental to magnetostriction [8].

These Fe-Ga alloys have the main advantage of being free of rare-earth elements and, thus, the cost is reduced compared to the rare-earth alloys family that has another drawback, which is their brittleness. The bulk Fe-Ga phase diagram is rich since many phases can coexist. Among them, on the Fe-rich side, one can cite the disordered bcc A2 phase, the ordered primitive cubic B2 phase, and the ordered DO_3 phase [9,10].

Fe-Ga alloys can be a good candidate to be associated with a piezoelectric material to form a composite multiferroic material. Such “extrinsic multiferroic” materials are

*jay@univ-brest.fr

an alternative path to the intrinsic multiferroics since only a few of the latter have high enough critical temperatures to be used in devices [11,12].

In composite materials, properties of each layer are combined: for example, magnetization can be controlled by an electric field through a strain transferred from the piezoelectric material to the magnetostrictive one. This is the converse magnetoelectric effect (CME), which can be schematically written as $CME = (\text{electric/mechanical}) \times (\text{mechanical/magnetic})$.

Moreover, such magnetic thin films are a very important part of flexible magnetoelectronics and an important foundation for the development of flexible magnetic devices [13,14].

For high-frequency devices, in-plane uniaxial anisotropy is needed. One way to adjust the anisotropy has been recently addressed in Fe-Ga alloy films (35 to 55 nm thick) deposited on lead magnesium niobate-lead titanate $Pb(Mg_{1/3} Nb_{2/3})O_3 - Pb(Ti)O_3$ piezoelectric substrates. Anisotropy is modified using both oblique incidence deposition and electric field [15].

A magnetoelectric composite composed of a layer of Fe-Ga alloy associated with a layer of lead zirconate titanate (piezoelectric ceramic material) Navy Type VI (PZT-5H) has been studied for potential applications in surgery such as cutting tools [16].

Clark *et al.* [17] have shown a nonmonotonic dependence of magnetostriction with Ga concentration with a double peak: the first one for 19% Ga content with $\frac{3}{2}\lambda_{100}$, reaching 400 ppm, and the other peak is close to 27%, with a slightly smaller magnetostriction coefficient. These authors have also shown a sharp change from $\frac{3}{2}\lambda_{111} \approx -20$ ppm to $\frac{3}{2}\lambda_{111} \approx +40$ ppm around 20% Ga alloy composition.

Very recently, it has been found that Fe-Ga single crystals alloys with specific thermal treatment behave in an unusual way: they show almost no magnetic hysteresis and these alloys are “non-Joulian”: their overall volume is not conserved during the magnetostriction process [18,19] contrary to the usual behavior when the material distorts in shape but not in volume since, while it expands in one direction, it contracts in the transverse directions. These alloys could find new applications in sensors and actuators. The magnetostrictive properties of Fe-Ga alloy depend strongly on composition preparation methods and thickness.

Previous works on thin films (thickness of 150 nm) have shown the same double-peaked maximum with Ga concentration as observed in bulk [20], but with lower magnetostriction values in 500-nm-thick films [21]. Javed *et al.* have studied the effect of sputtering deposition conditions on 50-nm-thick films with Ga concentration ranging from 19% to 23% and found a $\langle 110 \rangle$ crystallographic texture normal to the film plane and an effective saturation magnetostriction close

to 60 ppm [22]. Javed *et al.* also studied the thickness dependence (20–100 nm) of magnetostriction in a $Fe_{80}Ga_{20}$ polycrystalline alloy and determined the surface magnetostriction contribution [23].

Epitaxially grown $Fe_{81}Ga_{19}$ on Si/Cu with different thicknesses from 10 to 160 nm [24] or grown on MgO(100) with 90-nm-thickness films has also been studied [25].

Even if Fe-Ga alloy is widely studied within its film form, little emphasis has been given to a wide range of thickness-dependent magnetic properties. Extensive magnetization reversal and magnetostriction study for thin films thinner than 10 nm has only been reported seldomly [26,27]. In this paper, we report on an exhaustive magnetization reversal study with presentation of azimuthal behavior of the coercive field and the transverse magnetization. Samples with thicknesses ranging from 5 to 60 nm are deposited on glass substrates under a deposition field H_{dep} . Magnetostriction cycles are also presented for each thickness. These magnetic results are explored in correspondence with the structural study.

II. EXPERIMENTAL DETAILS

In this paper, a study of ultrathin $Fe_{81}Ga_{19}$ thin films grown by a sputtering technique is presented. $Fe_{81}Ga_{19}/Ta$ layers are grown by standard rf diode sputtering onto glass substrates (Schott D 263 TM [28]). A $Fe_{81\%}Ga_{19\%}$ target is used and the sample composition is checked with electron probe microanalysis (EPMA) measurements. The base pressure prior to the film deposition is typically 10^{-7} mbar. The ferromagnetic (FM) $Fe_{81}Ga_{19}$ thicknesses are $t_{FM} = 5, 10, 20,$ and 60 nm. Ta is used as a capping layer to protect the $Fe_{81}Ga_{19}$ from oxidation. The rf power used to sputter the 3-in. $Fe_{81}Ga_{19}$ target is 100 W and the argon pressure is 1.5×10^{-2} mbar. With these sputtering conditions, the growth rate is 0.22 nm s^{-1} . This rate is close to the one found by Weston *et al.* (0.3 nm s^{-1}) with quite similar deposition conditions [24].

An in-plane magnetic field of $H_{dep} \sim 2.4 \text{ kA m}^{-1}$ (300 Oe) is applied, during deposition, to induce a preferred direction. The influence of H_{dep} is discussed later in the paper. Structural analysis is performed by transmission electron microscopy (TEM) experiments on cross-sectional lamellas, thinned by mechanical polishing and argon ion milling at low temperature using a Gatan precision ion polishing system equipped with a liquid-nitrogen cooling system.

The samples are studied in high-resolution mode (the electron beam being parallel to a high symmetry axis of the crystal) in low magnification to ensure a large field of view. Selected-area diffracted patterns are recorded to evaluate the polycrystallinity of the layers as a function of their thickness.

X-ray measurements are performed with a four-circle X'Pert Pro Panalytical diffractometer, using a Cu K_{α} wavelength of 0.1542 nm, in a reflective mode.

Static magnetic measurements are performed at room temperature with a home-built vectorial vibrating sample magnetometer (VVSM), allowing us to determine both the longitudinal (M_L) and transverse (M_T) magnetization components. M_T is the magnetization component in the film plane, but perpendicular to H .

Coercive field temperature dependence is also obtained from $M(H)$ measurement using a Cryogenic cryogen-free physical properties measurement platform with a vibrating sample magnetometer inset. The magnet is initially demagnetized, after which the sample is cooled in zero applied magnetic field to the desired temperature. The $M(H)$ is then measured using the low-magnetic-field option of the Cryogenic system.

Magnetostriction is characterized using optical deflection. Under an applied magnetic field, the cantilever (made of glass substrate with $\text{Fe}_{81}\text{Ga}_{19}$ deposited onto it) deformation is recorded through laser beam reflection at the free tip. Further details can be found in a previous paper [29]. In thin films, since the magnetostrictive sample is grown onto a much thicker substrate, the magnetostrictive deformations are hindered by this substrate and one usually deals with the magnetoelastic coupling coefficient, b , rather than the magnetostriction coefficient, λ . This coefficient represents the characteristic magnetostrictive stress (see, for example, Ref. [29]). We check that the amplitude of the deflection (in absolute value) of the laser spot is unchanged whether it is reflected by the magnetic film of the sample or by the nonmagnetic film deposited from another side of the substrate.

III. XRD AND TEM CHARACTERIZATION

Crystallographic properties are first determined using x-ray diffraction as shown in Fig. 1. A very broad hump is observed around 20° that can be attributed to the x-ray signature of the amorphous glass substrate. A single Bragg peak is observed at 44.4° . This Bragg peak position corresponds to an interplanar spacing of 0.288 nm, which is in agreement with the results of Javed *et al.* for a 50-nm film [22], who noticed that the lattice parameter observed in such thin films is lower than those of thicker films or bulk values.

This Bragg peak position does not change for $\text{Fe}_{81}\text{Ga}_{19}$ thicknesses between 20 and 60 nm. It shows that the $\text{Fe}_{81}\text{Ga}_{19}$ crystallographic lattice does not evolve with thickness. Below 20 nm, it is not possible to measure clear XRD spectra because of the poor signal-to-noise ratio. It may be noted here that x-ray reflectivity is carried out on all samples to confirm the thicknesses. Nominal thicknesses appear to be very close to those determined by

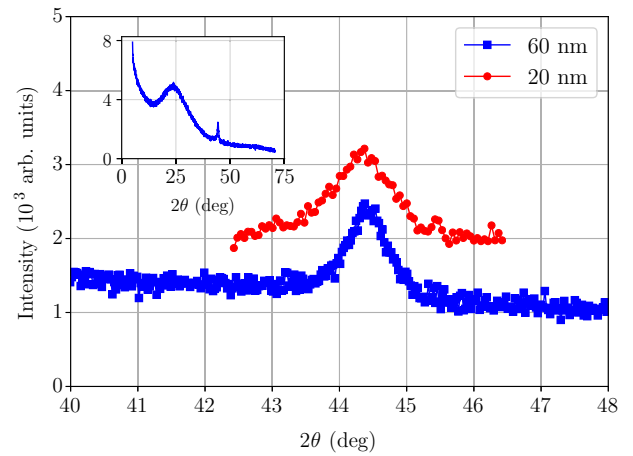


FIG. 1. $\theta - 2\theta$ pattern for 60- and 20-nm-thick $\text{Fe}_{81}\text{Ga}_{19}$ films. Inset: Full angle scan.

reflectivity. These x-ray spectra exhibit well-defined Kossel fringes in agreement with low-roughness thin films [30].

TEM characterization is carried out to probe the crystallographic properties for the thinnest films and also to determine the morphology of the films. TEM characterization is presented in Fig. 2 for the two samples of 7- and 40-nm thickness.

TEM images show that the thin films are continuous with the absence of holes and a low roughness for all thicknesses.

The diffraction patterns exhibit nonuniform circular rings with well-defined points or peaks present at some angular positions. Circular rings with a uniform distribution of intensity are a signature of polycrystalline crystallographic systems with no preferential orientation. However, the presence of well-defined spots in a diffraction pattern is characteristic of a well-defined long-range ordering encountered in epitaxial systems or substrates. The superposition of well-defined spots and circular rings therefore indicates that the thin films are composed of a polycrystalline fraction with no preferential orientation and another part of the volume that grows in a precise direction as in epitaxial systems [31,32]. The reinforcement of spot intensity in some directions is clear on the diffraction pattern corresponding to the thinnest sample, indicating a more “textured” film than the thicker one.

Such a fact may have critical consequences for the magnetic and magnetostrictive properties, which depend on the crystallographic arrangement, as shown later in this paper. In the following sections, the magnetic properties are analyzed using magnetometry and magnetostrictive techniques in light of the structural characterization presented in this section.

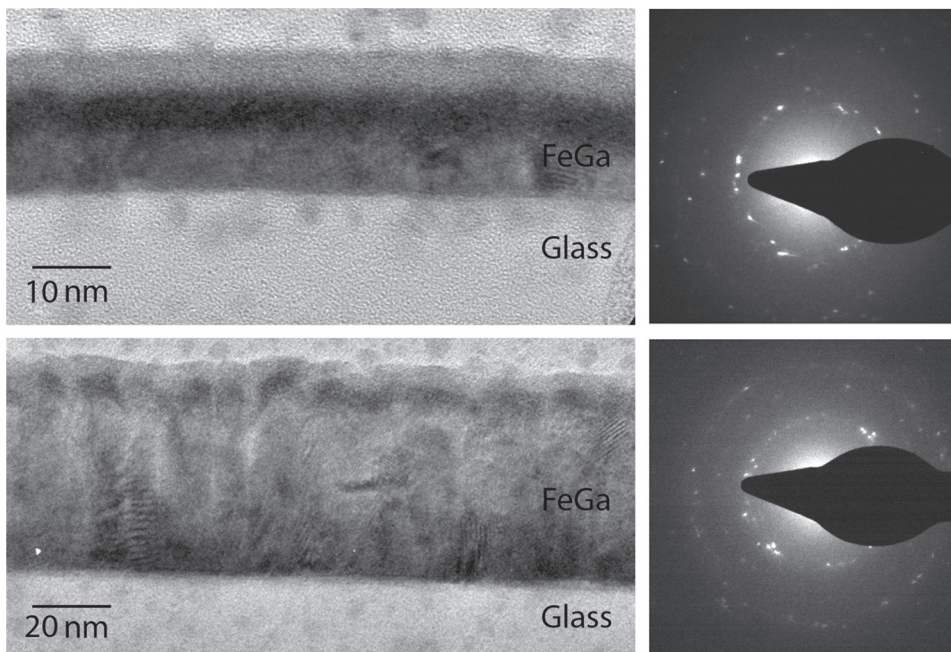


FIG. 2. High-resolution TEM image (left column: direct space; right column: reciprocal space) of a typical glass/Fe₈₁Ga₁₉(7 nm)/Ta bilayer is shown in the top image. The bottom figure shows the image obtained for the glass/Fe₈₁Ga₁₉(40 nm)/Ta thick film.

IV. MAGNETIZATION REVERSAL

Figure 3 shows the evolution of the saturation magnetic moment as a function of the Fe₈₁Ga₁₉ thickness. All the magnetic measurements are performed on samples with the same substrate surface area. The linear evolution of the saturation magnetic moment, thus, means that all samples from 5 to 60 nm have the same saturation magnetization $M_s = 919 \text{ kA m}^{-1}$ ($\mu_0 M_s = 1.15 \text{ T}$). This value is close to the one found by Zhang [33] for a 50-nm-thick Fe₈₁Ga₁₉ sample, but smaller than the one found by Gopman in thin films of thicknesses ranging from 20 to 80 nm [34] or in bulk materials that showed a saturation magnetization of 1.5 T.

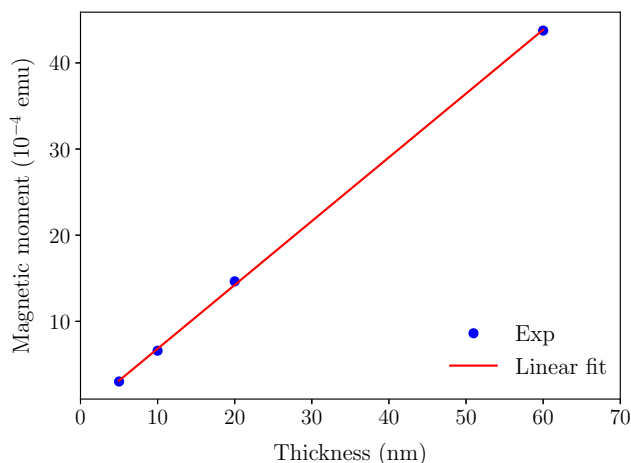


FIG. 3. Saturation magnetic moment as a function of Fe₈₁Ga₁₉ film thickness. The solid line is a linear fit.

Even though Endo *et al.* [26] have also observed a quasiconstant magnetization for Fe_{0.78}Ga_{0.22} films with thicknesses between 3 and 100 nm, it is quite remarkable that the magnetization for the present sample series remains constant for all thicknesses since a reduction of magnetization at the nanoscale may be observed when the thickness is decreased; i.e., reduction of the magnetization should be related to low dimensionality effects [35].

Figure 4 presents the magnetization hysteresis loops for the 5- and 60-nm samples for both transverse and longitudinal components. An in-plane magnetic field is applied along the direction of the applied deposition field ($\varphi = 0^\circ$) or perpendicularly to it ($\varphi = 90^\circ$). The third angle ($\varphi = 50^\circ$) corresponds to the maximum of $\text{Max}(M_T)/M_s$ found when varying φ (see Fig. 5).

For the 5-nm sample and along the $\varphi = 0$ direction, the transverse magnetization is flat, showing the absence of a net moment in the direction perpendicular to the applied field. Thus, the magnetization reversal is incoherent, involving domains nucleation and propagation. On the other hand, when external field is applied along the $\varphi = 50^\circ$ direction, the 5-nm normalized transverse magnetization shows a maximum value of 1, indicating a coherent magnetization reversal [i.e., a coherent (uniform) magnetization reversal] [36]. For larger thicknesses, the angular variation of transverse magnetization displays a similar behavior, in the sense of a maximum value at $\varphi = 50^\circ$. However, this M_T maximum value is reduced for thicker samples. It should be noted here that the observed angular dependence of the longitudinal and transverse components of magnetization does not correspond to a uniaxial anisotropic system with an easy axis induced by the applied field during growth. Indeed, such a uniaxial

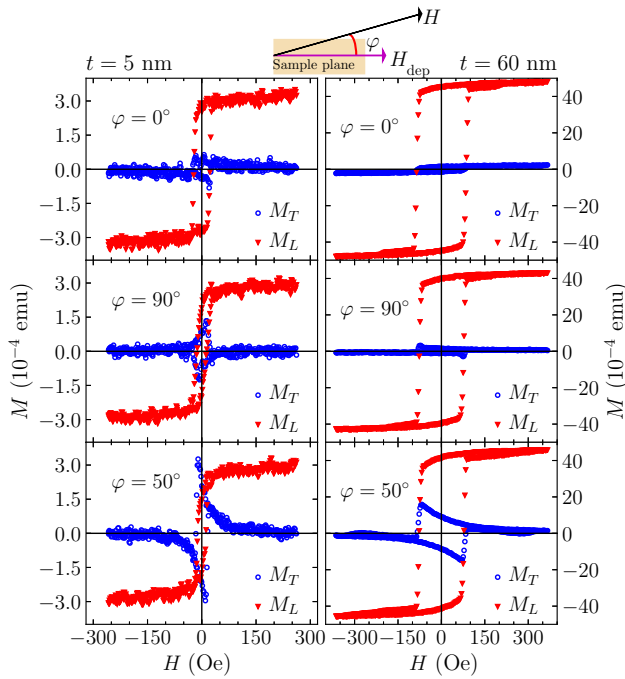


FIG. 4. In-plane magnetization loops of thickness 5 and 60 nm. Longitudinal M_L (red \blacktriangledown) and transverse M_T (blue \circ) components are shown. φ is the angle between the deposition axis and the direction of the in-plane applied field. $\varphi = 0$ corresponds to H applied parallel to the direction of the deposition field.

system would exhibit a maximum value of M_T perpendicular to the magnetic field applied during growth. In order to understand the driving mechanism for the magnetic properties' angular dependence, systematic in-plane azimuthal measurements are performed for all samples in increments of $\varphi = 10^\circ$. For each applied magnetic field direction, the maximum value of the transverse magnetization and the coercive field are obtained, as shown in Figs. 5 and 6.

Figure 5 shows the azimuthal angular dependence of the normalized (to the saturation magnetization M_s) maximum

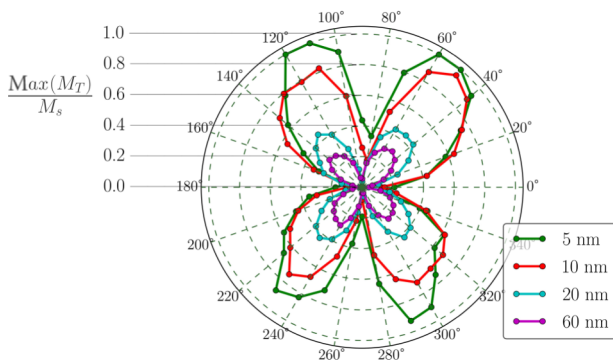


FIG. 5. Azimuthal behavior of the normalized maximum transverse magnetization, $\text{Max}(M_T)/M_s$, for different $\text{Fe}_{81}\text{Ga}_{19}$ film thicknesses.

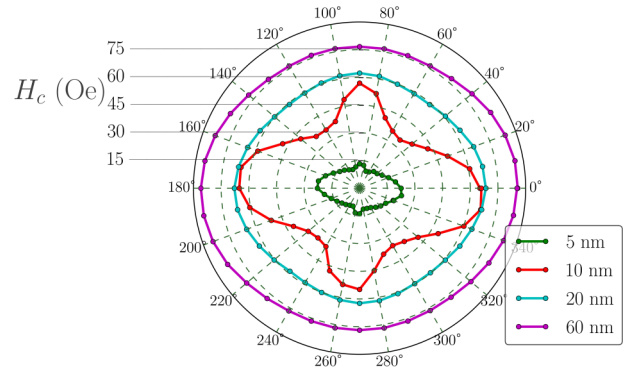


FIG. 6. Azimuthal behavior of the coercive field H_c for different $\text{Fe}_{81}\text{Ga}_{19}$ film thicknesses.

transverse magnetization $\text{Max}(M_T)/M_s$ for all samples. It reveals an “X” shape with four lobes and a well-defined symmetry: for a given thickness, the four lobes have the same size and their maxima show up at about 50° , 120° , 230° , and 300° with respect to the depositing field direction (i.e., 0°). Even though the lobe amplitude decreases when the thickness increases, it is worthwhile to note that their orientation does not vary with thickness. The symmetry of the azimuthal angular dependence for the transverse magnetization relates to the magnetic anisotropy present in a system. A uniaxial anisotropy system with coherent magnetization rotation, as described by the Stoner-Wohlfarth model [37], exhibits a well-known azimuthal shape of M_T , with two maxima. However, a magnetic system with a predominant cubic anisotropy exhibits an azimuthal shape with four maxima such as observed here. Furthermore, if the cubic anisotropy is of crystalline origin, then the maxima are related to the in-plane crystalline directions. Here, the angular positions of the maxima observed in Fig. 5 correspond to the angles between $[111]$ directions within the (110) plane in the cubic system.

Considering that the preferential growth discussed previously is along the $[110]$ directions, it shows that the crystalline ordering is the driving mechanism for ultrathin sputtered $\text{Fe}_{81}\text{Ga}_{19}$ systems studied here. $\text{Fe}_{81}\text{Ga}_{19}$ systems exhibit a magnetically hard axis along defined crystallographic directions. It favors a coherent rotation mechanism (i.e., a maximum of the transverse component) along these directions so as to minimize the anisotropic energy of the system. As already noted, the maxima orientation is not thickness dependent, whereas the maxima intensity decreases strongly with increasing thickness. It can be explained by an increase of the volume of the nonpreferential polycrystalline arrangement with increasing $\text{Fe}_{81}\text{Ga}_{19}$ thickness, as revealed by TEM observations. Therefore, this clearly demonstrates the presence of a surface anisotropy due to the low-dimensional effect in the rf sputtering ultrathin films. This surface anisotropy originates from the thickness-dependent crystallographic

texture effect. The same kind of anisotropy was observed by Weston *et al.* [24] in epitaxially grown $\text{Fe}_{81}\text{Ga}_{19}$ films with thicknesses ranging from 20 to 160 nm but not in sputtered ones: for very thin layers, Endo *et al.* have shown a small uniaxial anisotropy if $t \leq 7.5$ nm, but isotropic behavior above this thickness [26].

It is of interest to determine the angular dependence of the coercive field so as to further understand the effect of the magnetocrystalline component. The reason for this is because such a property is of prime interest for Fe-Ga alloy-based MEMS when studied in an external magnetic field [20].

Figure 6 shows a clear thickness dependence of the coercive field azimuthal shape. The thicker films exhibit a quasicircular (isotropic) shape, whereas the thinnest ones show a more complex behavior with local extrema positions reversed as compared to the M_T evolution. Thus, the directions of the H_c maxima correspond to M_T minima and vice versa. With increasing thickness, the maximum of H_c increases from 20 to 75 Oe. These values are of the same order as those found in $\text{Fe}_{81}\text{Ga}_{19}$ thin films grown epitaxially on Cu on Si [24], but at least half as small as the values found by Javed [22] in 50-nm-thick samples grown by cosputtering and evaporation techniques.

Zhang *et al.* [33] deposited a 50-nm-thick $\text{Fe}_{81}\text{Ga}_{19}$ onto a polyethylene terephthalate (PET) flexible substrate with varying Ta buffer layer thicknesses. They observed a uniaxial anisotropy decreasing with Ta thickness, attributed to residual stress from deformations in the PET substrate. Along the hard axis, the coercive field is reduced to 14 Oe when the Ta buffer layer is 20 nm. More recently, the same group studied wrinkled $\text{Fe}_{81}\text{Ga}_{19}$ films (20, 40, 60 nm) fabricated on elastic polydimethylsiloxane (PDMS) using two fabrication methods [38]. They found more or less uniaxial anisotropy depending on the fabrication methods and coercive field ranging from 40 to 90 Oe.

Finally, it should be noted that the minima of the coercive fields may be used in the future to minimize the external energy needed for controlling devices.

One may wonder what the influence of the deposition field H_{dep} is on the magnetic anisotropy character. A 5-nm-thick $\text{Fe}_{81}\text{Ga}_{19}$ sample is deposited in the exact same sputtering conditions but without H_{dep} . This sample is magnetically characterized in the same way as the 5-nm one deposited with H_{dep} . The same characteristic X shape of the azimuthal transverse magnetization with the same angles between the four lobes is found. Along the directions of these lobes, $\text{Max}(M_T)/M_s$ also reaches its maximum value of 1. The only difference we observe is a tilt (approximately 30°) in the whole polar plot. The deposition field H_{dep} thus orients the cubic anisotropy along a specific direction but does not modify the anisotropy type.

In order to complement this room-temperature magnetic study, coercive fields' dependence with temperature from 10 to 300 K is probed. This thermal behavior should be

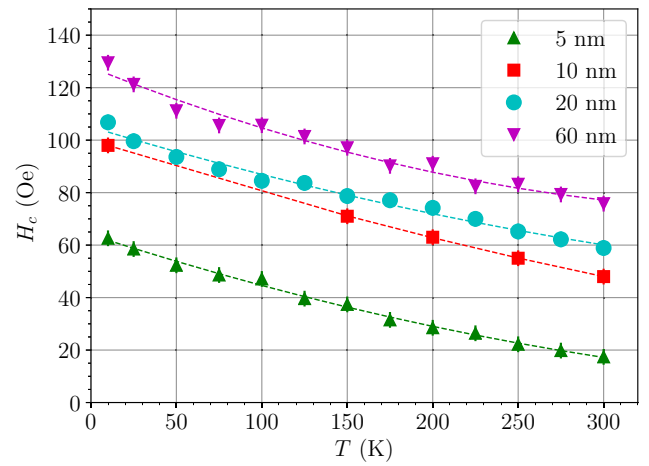


FIG. 7. Temperature evolution of the coercive field, H_c , for different $\text{Fe}_{81}\text{Ga}_{19}$ film thicknesses.

considered to understand the working temperature of sensor or actuator devices involving ultrathin Fe-Ga alloy films.

In order to measure the magnetization (M) of the $\text{Fe}_{81}\text{Ga}_{19}$ films as a function of applied magnetic field (H) at constant temperature, the following measurement protocol is used. The protocol starts with a demagnetization of the superconducting magnet, in order to obtain a zero magnetic field for the zero-field-cooled (ZFC) measurements. The sample is then cooled in zero field to the desired temperature and, after allowing the temperature to stabilize, $M(H)$ is then measured. After the $M(H)$ measurement, the system is heated back to 300 K, and then zero-field cooled again to the next desired temperature. This protocol is repeated in 25-K steps.

Coercive fields, H_c , as a function of temperature for all the samples are presented in Fig. 7. The usual decreasing H_c behavior with T is observed as also reported in CoCrTa films [39], in exchange-coupled NiFe/NiO layers [40], and in nanoparticles [41].

For all temperature ranges studied in this paper, the thinnest sample always has the smaller coercive field, while the thicker one has the most coercive one. The slopes of the coercive field as a function of temperature are roughly the same for all the thicknesses.

It indicates that there are no thickness-dependent magnetic phase transitions present in these $\text{Fe}_{81}\text{Ga}_{19}$ films.

V. MAGNETOSTRICTION

In a cubic crystal, the relative deformation due to magnetostriction is given by [42,43]

$$\frac{\delta \ell}{\ell} = \frac{3}{2} \lambda_{100} \left(\alpha_1^2 \beta_1^2 + \alpha_2^2 \beta_2^2 + \alpha_3^2 \beta_3^2 - \frac{1}{3} \right) + 3 \lambda_{111} (\alpha_1 \beta_1 \alpha_2 \beta_2 + \alpha_2 \beta_2 \alpha_3 \beta_3 + \alpha_1 \beta_1 \alpha_3 \beta_3), \quad (1)$$

where λ_{100} and λ_{111} are the saturation magnetostriction coefficients when the crystal is magnetized, and the strain is measured, in the directions $\langle 100 \rangle$ and $\langle 111 \rangle$, respectively [42]. α_i and β_i are respectively the direction cosines of the magnetization and observed elongation measured from cubic crystallographic directions ($[100]$, $[010]$, $[001]$). The magnetostrictive strain can also be expressed in terms of the tetragonal $\lambda^{t,2} = \frac{3}{2}\lambda_{100}$ and rhombohedral $\lambda^{r,2} = \frac{3}{2}\lambda_{111}$ magnetostriction constants, since an initially cubic cell magnetized along $[100]$ becomes slightly tetragonal, or rhombohedral when magnetized along $[111]$.

From Eq. (1), it is clear that $\delta\ell/\ell$ is sensitive to crystallinity and therefore different for monocrystalline, polycrystalline, or textured materials.

Let us call x the sample thickness, y the width, and z the length along which deformation is measured. When the magnetic field is rotated within the y - z plane, one can compute the azimuthal variation of deformation assuming that for strong enough magnetic fields, magnetization remains parallel to it. If φ is the angle measured from the sample length ($\varphi = 0$ when $\vec{H} \parallel z$ and $\varphi = 90^\circ$ when $\vec{H} \parallel y$), one gets the general formula for the (averaged where appropriate) relative deformation:

$$\frac{\delta\ell}{\ell} = A + B \cos(2\varphi), \quad (2)$$

where A and B are constants including both λ_{100} and λ_{111} with weighting coefficients depending on the crystallinity of the sample, as we show below for three simple cases.

In the case of a fully randomly oriented polycrystalline material, using Birss calculations [44] one finds $A = \frac{1}{10}\lambda_{100} + \frac{3}{20}\lambda_{111}$ and $B = \frac{3}{10}\lambda_{100} + \frac{9}{20}\lambda_{111}$.

In the case of a single crystal oriented such as $[110] \parallel x$, $[001] \parallel y$ and $[\bar{1}10] \parallel z$, one finds $A = -\frac{1}{8}\lambda_{100} + \frac{3}{8}\lambda_{111}$ and $B = \frac{3}{8}\lambda_{100} + \frac{3}{8}\lambda_{111}$.

In the case of a textured material with $[110] \parallel x$ and random orientations within the $(y-z)$ film plane, one finds $A = \frac{1}{16}\lambda_{100} + \frac{3}{16}\lambda_{111}$ and $B = \frac{9}{32}\lambda_{100} + \frac{15}{32}\lambda_{111}$.

In thin films, magnetostriction deformations are hindered by the much thicker substrate. In our experiment, we measure the bending angle $\theta(H)$ of the cantilever tip when the magnetic field is cycled from H_{\max} to $-H_{\max}$ and back to H_{\max} with $H_{\max} > H_{\text{sat}}$, where H_{sat} is the saturation field when magnetization reaches its saturation value [29]. In our experiment, H_{\max} is chosen as 1500 Oe. The bending angles $\theta(H)$ are converted to stress using the well-known formula [45]

$$b(H) = \frac{E_s t_s^2}{6(1 + \nu_s)L t_f} \times \theta(H), \quad (3)$$

where $E_s = 72.9$ GPa is the Schott D263 glass substrate Young modulus and $\nu_s = 0.208$ its Poisson ratio [28].

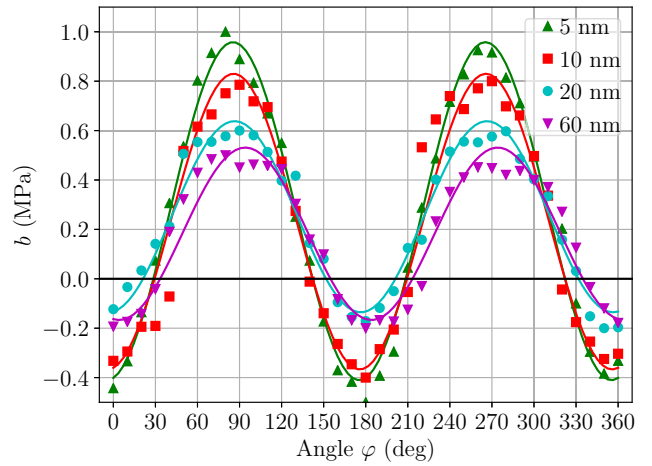


FIG. 8. Azimuthal behavior of magnetostriction for $t = 5, 10, 20, 60$ -nm-thick films. For each thickness, the solid line is a fit to experimental points using the function $A + B \cos(2\varphi + \delta)$.

The glass substrate thickness is $t_s = 30 \mu\text{m}$ and the $\text{Fe}_{81}\text{Ga}_{19}$ film thickness is t_f . L is the sample length (more precisely, the distance between the support and the laser spot on the sample). One can access the magnetostriction coefficient through $\lambda = -\frac{2}{3} \left[(1 + \nu_f) / E_f \right] \times b$, but the elastic coefficients of the thin film (ν_f and E_f) are needed. For very thin films, these elastic parameters are difficult to measure and usually stress b is considered as the relevant parameter for magnetostrictive effects. Nevertheless, following Hattrick-Simpers [21], we take $E_f / (1 + \nu_f) = 50$ GPa for $\text{Fe}_{81}\text{Ga}_{19}$ to compute λ and compare the values we get with those obtained by other authors.

The azimuthal behavior of b is shown in Fig. 8. The $\cos(2\varphi)$ (where φ is the angle between the applied magnetic field H and the cantilever length) expected behavior [see Eq. (2)] is found for all sample thicknesses.

The full H -bending cycles for the two remarkable angles $\varphi = 0$ (\parallel cantilever length and deposition field) and $\varphi = 90^\circ$ (\perp) are shown in Fig. 9.

To access the effective magnetostriction constant (λ_{eff}) or the characteristic magnetostrictive stress (b_{eff}), one has to perform at least two measurements: along the sample length (parallel) and along the sample width (perpendicular), since the magnetostriction constant is given by [42,46] $\lambda_{\text{eff}} = \frac{2}{3} [(\delta\ell/\ell)_{\parallel} - (\delta\ell/\ell)_{\perp}]$ and similarly $b_{\text{eff}} = b_{\parallel} - b_{\perp}$. Obviously, magnetostriction can also be deduced from the azimuthal behavior of b , i.e., the $\cos(2\varphi)$ amplitude as seen in Fig. 8.

One should notice that b_{eff} is negative for these $\text{Fe}_{81}\text{Ga}_{19}$ samples. This corresponds to a positive magnetostriction since the magnetostriction coefficient λ and b are related through a negative coefficient and thus a dilation along the applied field direction.

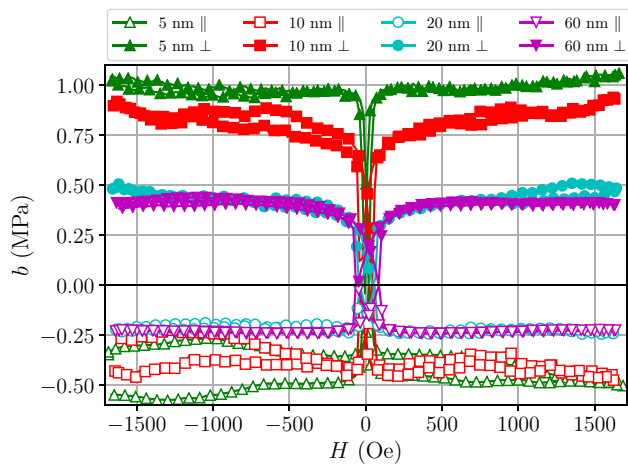


FIG. 9. Magnetostrictive bending H cycles of $\text{Fe}_{81}\text{Ga}_{19}$ cantilever films for thicknesses $t = 5, 10, 20, 60$ nm. Magnetic field is applied either parallel to the cantilever length (\parallel) or perpendicular to it (\perp).

Figure 9 shows the bending H cycles for the different sample thicknesses. The coercive field enhancement already seen with increasing thickness (measured from $M - H$ VSM loops and shown in Fig. 7) is also visible on the magnetostriction cycles. Indeed, the magnetostrictive loops widen when thickness increases and the coercive field corresponds to the field when b switches to 0.

The evolution of $|b_{\text{eff}}|$ and λ_{eff} with film thickness is presented in Fig. 10, which shows that $|b|$ is thickness dependent, since $|b_{\text{eff}}|$ (λ) decreases from 1.5 to 0.7 MPa (from 20 to 9 ppm) when t increases from 5 to 60 nm.

When decreasing thickness, our structural and magnetic studies show that sample texture increases. This structural modification impacts λ_{eff} since the weighting coefficients of λ_{100} and λ_{111} appearing in A and B in Eq. (2)

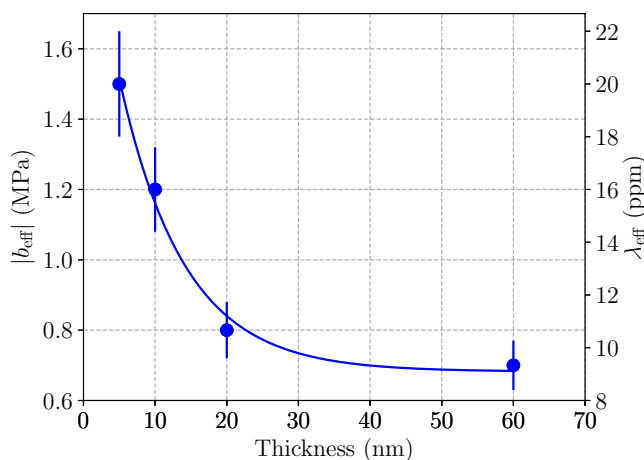


FIG. 10. Evolution of the magnetoelastic coefficient, $|b_{\text{eff}}|$, and magnetostriction coefficient, λ_{eff} , with $\text{Fe}_{81}\text{Ga}_{19}$ thickness. The solid line is a guide for the eye.

are crystallinity dependent. Yet it is not possible to exactly determine these coefficients since precise crystallography and orientations are not accurately known. However, the difference between the thinnest sample (5 nm) and the thicker samples cannot exclusively be explained by this effect.

In fact, for very thin samples, the proportion of interface and surface atoms with obviously different symmetry from bulk atoms is large. Thus, this may contribute differently to magnetostriction, as observed in anisotropy where a surface term is usually added to the bulk one when the film is only constituted of a few atomic planes. Similarly to the anisotropy phenomenological expression, one can write $\lambda_{\text{eff}} = \lambda_{\text{bulk}} + \lambda_{\text{surf}}/t$, as suggested by Néel [47] and Szymczak [48]. Once again, the thickness evolution obtained in the present study cannot be explained alone by only considering the surface contribution. It would be hazardous to extract λ_{bulk} and λ_{surf} from the present data since varying the thickness modifies the crystallinity. The evolution of magnetostriction with thickness is probably a combination of both crystallinity and surface effects.

The order of magnitude obtained in the present investigation for magnetostriction is comparable with the value found by other authors for comparable Ga alloy concentrations (20%), but the thickness evolutions are rather different according to various studies: Javed *et al.* [23] found an increase of λ_{eff} from approximately 20 to 80 ppm when t increases from 20 to 100 nm in $\text{Fe}_{80}\text{Ga}_{20}$. Yu *et al.* [49] showed that magnetostriction decreases from 35 to 28 ppm when thickness increases from 10 to 120 nm.

For very thin $\text{Fe}_{78}\text{Ga}_{22}$ samples (3–10 nm), Endo *et al.* [26] reported a magnetostriction fluctuation between 15 and 20 ppm, reaching 24 ppm for 30 nm and then decreasing to 18 ppm at 100 nm.

For a $\text{Fe}_{81}\text{Ga}_{19}$ 110-nm-thick film deposited on glass, Jen *et al.* [50] found $\lambda_s = 21$ ppm, a very close value to that measured by Yu *et al.* in a sample deposited onto a flexible PET substrate [13]. Thus, the value obtained in the present study for the magnetostriction corresponds well with that previously reported in the literature.

VI. CONCLUSION

We perform an exhaustive magnetization reversal study on $\text{Fe}_{81}\text{Ga}_{19}$ samples with thicknesses ranging from 5 to 60 nm. The magnetic results including magnetostriction cycles are explored in light of a structural study.

We show that thin $\text{Fe}_{81}\text{Ga}_{19}$ films deposited by sputtering exhibit peculiar anisotropy directions even if growth is initiated onto an amorphous glass substrate. The deposition field H_{dep} orients the anisotropy along a specific direction but is not necessary to induce the observed anisotropy.

This anisotropy revealed by XRD and TEM is prominent for the thinnest films ($t \leq 10$ nm) and has clear consequences for magnetic and magnetostrictive behaviors:

when rotating the applied magnetic field in the film plane, transverse magnetization is maximum for specific directions. Angles between these directions correspond to the [111] family directions in-between angles in the (110) plane. Thus, when external field is applied along these specific directions, magnetization reversal is mainly coherent. The present study also shows that magnetostriction coefficient is higher for the thinnest samples (5 nm), where the polycrystalline part of the sample is reduced as compared to the thicker one (60 nm). We demonstrate that the thinnest film possesses the best characteristics for potential applications: highest magnetostriction coefficient, lowest coercive and saturation fields, and pronounced anisotropy. Film thickness thus strongly affects the magnetic and magnetostrictive properties of Fe₈₁Ga₁₉ films. It has to be taken into account for applications when anisotropy is required, such as in microwave devices.

Good magnetic characteristics found in the 5-nm-thick film are also desired when this magnetostrictive alloy is associated with a piezoelectric material so as to form an extrinsic multiferroic composite. Voltage control of magnetism through strain-mediated magnetoelectric coupling between the piezoelectric material and the magnetostrictive one is a key function in magnetic memory and logic devices.

ACKNOWLEDGMENTS

Région Bretagne is acknowledged for ARED support (partial W.J. Ph.D. financial support). This work is supported by the South African National Research Foundation Grants No. 80928, No. 93551, No. 115346, and No. 80880 and the URC and FRC of the University of Johannesburg, South Africa.

-
- [1] C. Mudivarthi, S. Datta, J. Atulasimha, P. G. Evans, M. J. Dapino, and A. B. Flatau, Anisotropy of constrained magnetostrictive materials, *J. Magn. Magn. Mater.* **322**, 3028 (2010).
- [2] S. U. Jen, and C. C. Liu, Magneto-elastic and magnetic domain properties of Fe₈₁Ga₁₉/Si(100) films, *J. Appl. Phys.* **115**, 013909 (2014).
- [3] K. Roy, S. Bandyopadhyay, and J. Atulasimha, Hybrid spintronics and straintronics: A magnetic technology for ultra low energy computing and signal processing, *Appl. Phys. Lett.* **4**, 063108 (2011).
- [4] H. Ahmad, J. Atulasimha, and S. Bandyopadhyay, Reversible strain-induced magnetization switching in FeGa nanomagnets: Pathway to a rewritable, non-volatile, non-toggle, extremely low energy straintronic memory, *Sci. Rep.* **5**, 18264 (2015).
- [5] W. Li, B. Buford, A. Jander, and P. Dhagat, Acoustically Assisted Magnetic Recording: A New Paradigm in Magnetic Data Storage, *IEEE Trans. Magn.* **50**, 37 (2014).
- [6] A. E. Clark, J. B. Restorff, M. Wun-Fogle, T. A. Lograsso, and D. L. Schlager, Magnetostrictive properties of body-centered cubic Fe-Ga and Fe-Ga-Al alloys, *IEEE Trans. Magn.* **36**, 3238 (2000).
- [7] J. Atulasimha, and A. B. Flatau, A review of magnetostrictive iron-gallium alloys, *Smart Mater. Struct.* **20**, 043001 (2011).
- [8] T. A. Lograsso, A. R. Ross, D. L. Schlager, A. E. Clark, and M. Wun-Fogle, Structural transformations in quenched Fe-Ga alloys, *J. Alloys Compd.* **350**, 95 (2003).
- [9] H. Okamoto, The Fe-Ga (iron-gallium) system, *J. Phase Equilib.* **11**, 576 (1990).
- [10] O. Ikeda, R. Kainuma, I. Ohnuma, K. Fukamichi, and K. Ishida, Phase equilibria and stability of ordered bcc phases in the Fe-rich portion of the FeGa system, *J. Alloys Compd.* **347**, 198 (2002).
- [11] D. E. Parkes, L. R. Shelford, P. Wadley, V. Holý, M. Wang, A. T. Hindmarch, G. van der Laan, R. P. Campion, K. W. Edmonds, S. A. Cavill, and A. W. Rushforth, Magnetostrictive thin films for microwave spintronics, *Sci. Rep.* **3**, 2220 (2013).
- [12] N. A. Spaldin, and R. Ramesh, Advances in magnetoelectric multiferroics, *Nat. Mater.* **18**, 10 (2019).
- [13] Y. Yu, Q. Zhan, J. Wei, J. Wang, G. Dai, Z. Zuo, X. Zhang, Y. Liu, H. Yang, Y. Zhang, S. Xie, B. Wang, and R.-W. Li, Static and high frequency magnetic properties of FeGa thin films deposited on convex flexible substrates, *Appl. Phys. Lett.* **106**, 162405 (2015).
- [14] P. Sheng, B. Wang, and R. Li, Flexible magnetic thin films and devices, *J. Semicond.* **14**, 011006 (2018).
- [15] Y. Zhang, C. Huang, M. Turghun, Z. Duan, F. Wang, and W. Shi, Electric-regulated enhanced in-plane uniaxial anisotropy in FeGa/PMN-PT composite using oblique pulsed laser deposition, *Appl. Phys. A* **124**, 289 (2018).
- [16] Y. Wang, J. Atulasimha, J. Clarke, and V. B. Sundaresan, in *Behavior and Mechanics of Multifunctional Materials and Composites 2010* (International Society for Optics and Photonics, San Diego, California, United States, 2010), Vol. 7644, p. 764414.
- [17] A. E. Clark, K. B. Hathaway, M. Wun-Fogle, J. B. Restorff, T. A. Lograsso, V. M. Keppens, G. Petculescu, and R. A. Taylor, Extraordinary magnetoelasticity and lattice softening in bcc Fe-Ga alloys, *J. Appl. Phys.* **93**, 8621 (2003).
- [18] H. D. Chopra, and M. Wuttig, Non-Joulian magnetostriction, *Nature* **521**, 340 (2015).
- [19] R. D. James, Materials science: Magnetic alloys break the rules, *Nature* **521**, 298 (2015).
- [20] R. Basantkumar, B. Stadler, W. Robbins, and E. Summers, Integration of Thin-Film Galfenol With MEMS Cantilevers for Magnetic Actuation, *IEEE Trans. Magn.* **42**, 3102 (2006).
- [21] J. R. Hatrick-Simpers, D. Hunter, C. M. Craciunescu, K. S. Jang, M. Murakami, J. Cullen, M. Wuttig, I. Takeuchi, S. E. Lofland, L. Benderksy, N. Woo, R. B. Van Dover, T. Takahashi, and Y. Furuya, Combinatorial investigation of magnetostriction in Fe-Ga and Fe-Ga-Al, *Appl. Phys. Lett.* **93**, 102507 (2008).
- [22] A. Javed, N. Morley, and M. Gibbs, Structure, magnetic and magnetostrictive properties of as-deposited Fe-Ga thin films, *J. Magn. Magn. Mater.* **321**, 2877 (2009).

- [23] A. Javed, N. A. Morley, and M. R. J. Gibbs, Thickness dependence of magnetic and structural properties in $\text{Fe}_{80}\text{Ga}_{20}$ thin films, *J. Appl. Phys.* **107**, 09A944 (2010).
- [24] J. Weston, A. Butera, T. Lograsso, M. Shamsuzzoha, I. Zana, G. Zangari, and J. Barnard, Fabrication and characterization of $\text{Fe}_{81}/\text{Ga}_{19}$ thin films, *IEEE Trans. Magn.* **38**, 2832 (2002).
- [25] A. Butera, J. Gómez, J. L. Weston, and J. A. Barnard, Growth and magnetic characterization of epitaxial $\text{Fe}_{81}\text{Ga}_{19}$ $\text{MgO}(100)$ thin films, *J. Appl. Phys.* **98**, 033901 (2005).
- [26] Y. Endo, T. Sakai, T. Miyazaki, and Y. Shimada, Effect of Film Thickness on the High Frequency Magnetic Properties of Polycrystalline Fe–Ga Films, *IEEE Trans. Magn.* **53**, 5 (2017).
- [27] Y. Yu, S. Xie, and Q. Zhan, Effect of Thickness on Mechanically Tunable Magnetic Anisotropy of FeGa Thin Films Deposited on Flexible Substrates, *Mater. Sci. Forum* **815**, 227 (2015).
- [28] Schott website, https://www.schott.com/nexterion/english/products/uncoated-substrates/d263.html?highlighted_text=d263.
- [29] J. P. Jay, F. Le Berre, S. P. Pogossian, and M. V. Indenbom, Direct and inverse measurement of thin films magnetostriction, *J. Magn. Magn. Mater.* **322**, 2203 (2010).
- [30] E. Hecht, *Optics* (Addison-Wesley, 1987).
- [31] J. Richy, T. Hauguel, J.-P. Jay, S. P. Pogossian, B. Warot-Fonrose, C. J. Sheppard, J. L. Snyman, A. M. Strydom, J. B. Youssef, A. R. E. Prinsloo, D. Spenato, and D. T. Dekadjevi, Temperature dependence of exchange biased multiferroic $\text{BiFeO}_3/\text{Ni}_{81}\text{Fe}_{19}$ polycrystalline bilayer, *J. Phys. D: Appl. Phys.* **51**, 125308 (2018).
- [32] G. Cappuccio, and M. L. Terranova, Thin Film Characterisation by Advanced X-Ray Diffraction Techniques, type Tech. Rep. number LNF-IR-96-049 (Istituto Nazionale di Fisica Nucleare, 1996).
- [33] X. Zhang, Q. Zhan, G. Dai, Y. Liu, Z. Zuo, H. Yang, B. Chen, and R.-W. Li, Effect of buffer layer and external stress on magnetic properties of flexible FeGa films, *J. Appl. Phys.* **113**, 17A901 (2013).
- [34] D. B. Gopman, V. Sampath, H. Ahmad, S. Bandyopadhyay, and J. Atulasimha, Static and Dynamic Magnetic Properties of Sputtered Fe–Ga Thin Films, *IEEE Trans. Magn.* **53**, 1 (2017).
- [35] C. Le Graët, D. Spenato, N. Beaulieu, D. T. Dekadjevi, J.-P. Jay, S. P. Pogossian, B. Warot-Fonrose, and J. Ben Youssef, Driving mechanism for damping and g-factor in non-amorphous ferromagnetic CoFeZr ultrathin films, *Europhys. Lett.* **115**, 17002 (2016).
- [36] D. J. Sellmyer, C. P. Luo, Y. Qiang, and J. P. Liu, in *Handbook of Thin Films*, edited by H. Singh Nalwa (Academic Press, Burlington, 2002), p. 337.
- [37] E. C. Stoner, and E. P. Wohlfarth, A mechanism of magnetic hysteresis in heterogeneous alloys, *Phil. Trans. R. Soc. Lond. A* **240**, 599 (1948).
- [38] S. Zhang, Q. Zhan, Y. Yu, L. Liu, H. Li, H. Yang, Y. Xie, B. Wang, S. Xie, and R.-W. Li, Surface morphology and magnetic property of wrinkled FeGa thin films fabricated on elastic polydimethylsiloxane, *Appl. Phys. Lett.* **6**, 102409 (2016).
- [39] H. Zeng, Z. Shan, Y. Liu, M. Azarisooreh, K. Honardoost, and D. Sellmyer, Studies of the magnetic and reversal properties for thin CoCrTa films, *J. Magn. Magn. Mater.* **251**, 283 (2002).
- [40] D. T. Dekadjevi, A. R. E. Prinsloo, E. Carleschi, J. Richy, C. Legraet, S. P. Pogossian, J.-P. Jay, D. Spenato, J. Ben Youssef, and A. M. Strydom, Driving the magnetization reversal below the blocking temperature in exchange biased NiFe/NiO , *J. Appl. Phys.* **114**, 093904 (2013).
- [41] W. C. Nunes, W. S. D. Folly, J. P. Sinnecker, and M. A. Novak, Temperature dependence of the coercive field in single-domain particle systems, *Phys. Rev. B* **70**, 014419 (2004).
- [42] B. D. Cullity, and C. D. Graham, *Introduction to magnetic materials* (IEEE/Wiley, NJ, 2009), 2nd ed.
- [43] G. Petculescu, R. Wu, and R. McQueeney, in *Handbook of Magnetic Materials* (Amsterdam, The Netherlands, Elsevier), Vol. 20, p. 123.
- [44] R. R. Birss, The Saturation Magnetostriction of Polycrystals, *Proc. Phys. Soc.* **75**, 8 (1960).
- [45] E. d. T. d. Lacheisserie, and J. C. Peuzin, Magnetostriction and internal stresses in thin films: the cantilever method revisited, *J. Magn. Magn. Mater.* **136**, 189 (1994).
- [46] M. Kaneko, S. Hashimoto, M. Hayakawa, and K. Aso, Measuring the magnetostriction of thin films using an optical displacement meter, *J. Phys. E Sci. Instrum.* **21**, 487 (1998).
- [47] L. Néel, Anisotropie magnétique superficielle et surstructures d'orientation, *J. Phys. Radium* **15**, 225 (1954).
- [48] H. Szymczak, and R. Żuberek, Surface Magnetostriction, *Acta Phys. Pol. A* **83**, 651 (1993).
- [49] Y. Yu, S. H. Xie, and Q. F. Zhan, Effect of Thickness on Mechanically Tunable Magnetic Anisotropy of FeGa Thin Films Deposited on Flexible Substrates, *Mater. Sci. Forum* **815**, 227 (2015).
- [50] S. U. Jen, C. C. Liu, and C. Y. Chuang, Magneto-elastic and mechanical properties of $\text{Fe}_{81-x}\text{Ni}_x\text{Ga}_{19}/\text{Si}(100)$ and $\text{Fe}_{81-y}\text{Ni}_y\text{Ga}_{19}/\text{glass}$ films, *Adv. Mat. Res.* **705**, 66 (2013).